Ab initio and experimental pre-edge investigations of the Mn *K*-edge XANES in oxide-type materials

François Farges*
Laboratoire des géomatériaux, Université de Marne-la-Vallée, CNRS FRE 2455, 77454 Marne la Vallée Cedex, France and Department of Geological and Environmental Sciences, Stanford University, Stanford, California 94305-2115, USA
(Received 1 September 2004; revised manuscript received 26 October 2004; published 15 April 2005)

Mn *K* edge *ab initio* FEFF8.2 calculations of the pre-edge features of the x-ray-absorption near-edge structure (XANES) region were undertaken for a series of Mn-bearing oxide-type compounds. The aim of the study is to provide a reliable method for determining quantitative and accurate redox and symmetry information for manganese. In agreement with multiplet calculations by Glatzel and co-workers, FEFF8.2 predicts a doublet and a triplet for Mn(II) and Mn(III) in octahedral symmetry, respectively, in agreement with high-resolution XANES experiments. Site distortion increases notably the contribution from dipolar transitions and, consequently, the pre-edge feature integrated area. An even more intense pre-edge feature is calculated and measured for the T_d symmetry (singletlike). For Mn(IV), a triplet is predicted and measured for the O_h symmetry. However, additional transitions are found in Mn(IV)-rich compounds, that are related to metal-metal transitions. These transitions overlap strongly with the "true pre-edge," making extraction of redox and symmetry information for Mn(IV) more challenging. However, a model of the pre-edge with pseudo-Voigt functions of fixed calculated width (based on core-hole lifetime and experimental resolution) helps to separate the contributions related to first-neighbor symmetry from those of the metal-metal pairs. Application to multivalent defective manganese oxide materials suggests that the pre-edge information varies linearly as a function of Mn redox state or symmetry but varies nonlinearly as a function of both parameters. Finally, the polymerization of the manganese networks can be estimated from the metal-metal transitions found in the pre-edge region.

DOI: 10.1103/PhysRevB.71.155109 PACS number(s): 61.10.Ht, 31.15.Ar, 31.70.−f, 78.55.Qr

I. INTRODUCTION

Manganese redox states range from 0 to +7. Among them, the divalent, trivalent, and tetravalent are the most commonly encountered redox states in industrial, geological, chemical, or biological materials.[1,2] In a number of Mn-bearing phases (such as Mn_3O_4),[3] several redox states of manganese can coexist (multivalency). Concomitant charge compensation (or charge disproportionation as in manganite-type compounds) occurs thanks to other cationic substitutions (often iron, alkali metals, and hydrogen). These redox equilibria often occur in a variety of Mn-rich oxides, such as the α-MnO_2–δ-MnO_2 family of manganese dioxides, as well as layered defective phyllomanganates.[2–4] These last phases are important constituents of soils as well as polymetallic nodules found in oceans,[5–9] but also in biological systems (such as bacterial),[10–14] in particles emitted by manganese-bearing gasolines,[15] or in nuclear waste glasses,[16] whose impact on toxicology makes x-ray-absorption near-edge structure (XANES) a well-suited tool.[17]

Therefore, x-ray-absorption fine structure (XAFS) spectroscopy has been widely used to study the local structure around manganese in these oxide-based systems with the aim, among others, to measure directly the redox state of manganese in a variety of inorganic[3–9,14,18–21] and bio-inorganic systems,[18–21] but also in historical artifacts.[22–24] Hence, many authors have reported a shift of the edge position (measured either at the inflection point or "halfway") for a systematically limited selection of models compounds of manganese.[4,7,12,16] However, a Mn *K* edge XANES study of a more representative set of model compounds[24,25] reveals a more complex situation, making the previously published studies on Mn redox estimation not applicable anymore. For instance, Fig. 1(a) shows two quite different compounds (MnO and $MnCO_3$) which share the same manganese redox state and coordination [i.e., Mn(II) in O_h]. The extraction of the redox information is impossible from the edge energy position (using either the edge crest, the first derivative, or the "halfway" E_0 value) because of the edge separation of $\sim$4.5 eV between both compounds. Constructive and destructive interferences (single and multiple scattering) arising from more distant neighbors around the central manganese atoms are at the origin of the large variations in the Mn *K* edge XANES spectra of MnO and $MnCO_3$ [Fig. 1(d)]. For instance, *ab initio* FEFF8.2 calculations for MnO [Fig. 1(d); structure information from Ref. 1] suggest that a $\sim$2 eV shift in the Mn *K* edge position (measured either at the edge crest or within the edge jump) is related to the 36 distant manganese neighbors, located between 5 and 6.5 Å from the central Mn.[1] Consequently, correlating between the edge position and redox state of Mn is feasible only when the number of models is restricted to a small number of closely related compounds (such as MnO, Mn_3O_4, Mn_2O_3 and β-MnO_2 for instance).[16] However, the measurement of the edge energy for a large selection of highly diverse model compounds [such as the ones presented here; see Fig. 1(b)] shows that the correlation between redox state and edge position, although positive, is far from accurate (the correlation coefficient r^2 is only 0.95). This is particularly true for Mn(II)- and Mn(IV)-bearing compounds, whose edge positions can vary by more than 6 eV (resulting in error bars in redox determination of up to 90%).

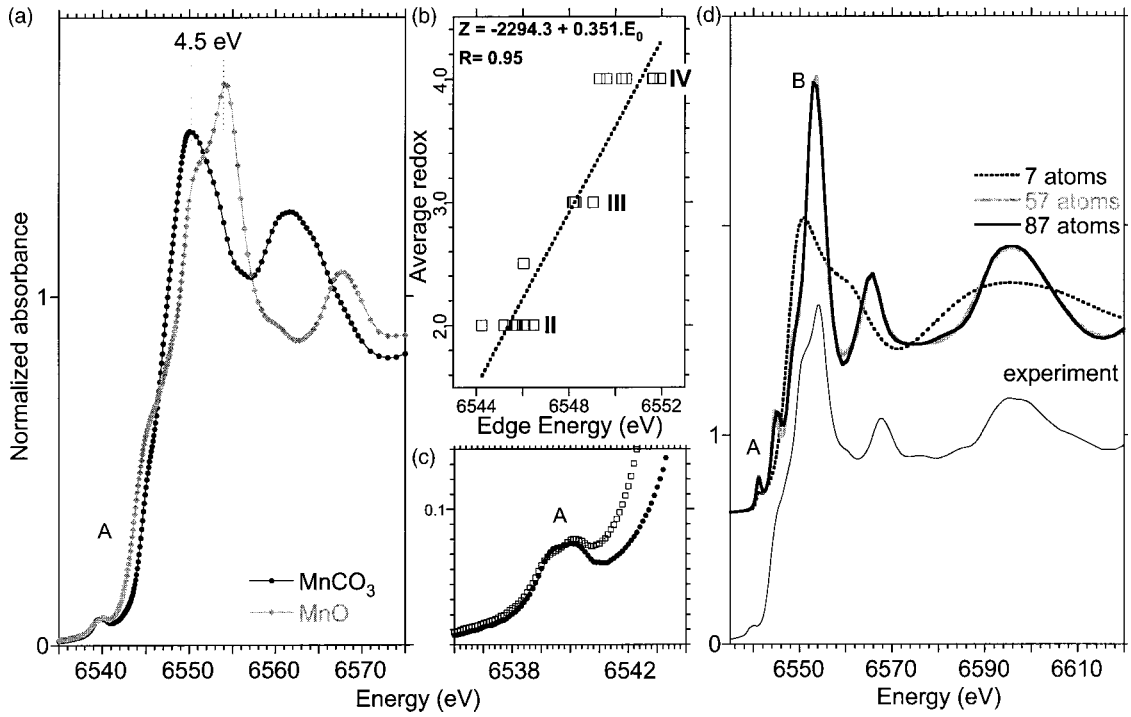

FIG. 1. Normalized Mn *K* edges for MnO and $MnCO_3$ (a), in which Mn(II) is located in O_h sites, showing their differences in the main edge region; (b) plot of the "halfway" edge E_0 energy for the different models of this study as a function of their Mn redox state, showing a positive trend but not accurate enough to be quantitative; (c) detail of the pre-edge region shown in (a), showing the good recurrence of this feature for constant symmetry.

Consequently, a more robust approach to deriving Mn redox information is needed, such as that provided by the study of the pre-edge feature at the Mn *K* edge. The pre-edge feature of the *K* edge of manganese is located ~15–20 eV before the main *K* edge crest of manganese. The pre-edge feature is related to electronic transitions from the 1*s* core levels to the empty 3*d* levels, more or less 4*p* hybridized by the Mn ligands (probing thus the density of the lowest unoccupied states). This pre-edge feature appears much less affected by changes in the medium- and long-range environment than the main edge region [Fig. 1(c)]. As shown previously,[8,18–21,23,24,26–34] pre-edge features are a potentially useful indicator of the redox state and symmetry (through their energy and relative area). However, some authors have pointed out already the difficulty in extracting redox information from the pre-edge features at the Mn *K* edge.[20] This limitation was partially overcome recently, thanks to theoretical calculations, using either the multiplet theory[26,27] or multiple-scattering calculations (using FEFF8.2).[16,19,27] However, these last studies did not explicitly take quadrupolar transitions into account, although these transitions are crucial to describe properly the pre-edge region, particularly for centrosymetric sites.[28–30] In parallel, the collection of resonant inelastic x-ray scattering (RIXS) spectra (together with multiplet calculations) on selected model compounds[21,31,32] definitively shed an important light on the detailed structure of the pre-edge feature of the Mn *K* edge. Indeed, these studies provide information on the number, position, and relative intensities of each transition that must be modeled in the pre-edge region collected at the Mn *K* edge. However, the influence of dipolar-dominant transitions (as under T_d geometry) cannot be tested using multiplets, nor the influence of metal-metal transitions.[33,34] The use of a one-electron theory, as in FEFF8.2,[35,36] is a complementary tool to multiplet calculations, despite its own intrinsic limitations (lack of multielectronic effects, other many-body effects can be lumped into phenomenological broadening, the overlapping of atom potentials and the use of the spherical muffin-tin approximation, the poor estimates of Debye-Waller factors, etc.).

In this study, the results of Mn *K* edge FEFF8.2 calculations are presented, thanks to the release of the latest version of FEFF8.2, which added (among other features) the possibility to calculate quadrupolar transitions.[36] The effects of dipolar and quadrupolar transitions are examined together with the influence of site symmetry (including site distortion) and contributions from next-nearest neighbors. The data are compared to a high-resolution XANES spectroscopy study collected for a set of well-characterized manganese-bearing model compounds, in which manganese exhibits redox states ranging from 2 to 4. These samples include numerous oxides and silicates, natural or synthetic, and well characterized.

II. EXPERIMENT

A. *Ab initio* calculations

The FEFF8.2 (#9 or "final") code[35,36] was chosen, using as many default parameters as possible, such as the use of the Hedin-Lunqvist self-consistent potentials (EXCHANGE 0 0), the muffin-tin approximation with automatic overlapping (AFOLP), and default values for the angular momentum for each atom type (l=−1). However, dipolar and quadrupolar

TABLE I. Pre-edge information for the models for Mn(II). The asterisk indicates convergence to a null integrated area.

	Pseudo-Voigt function			
Sample	Energy (eV)	Integrated area	Centroid (eV)	Total integrated area
$MnFe_2O_4$	6540.63	0.176	6540.65	0.185
Jacobsite, synthetic	6540.95	0.009		
	*	*		
$(Mn,Ni)Cr_2O_4$	6540.57	0.198	6540.66	0.224
Manganonichromite, synthetic	6541.39	0.026		
	*	*		
$(Fe,Mn)_2Al_9O_7(SiO_4)_4(OH)$	6539.56	0.013	6540.59	0.191
Staurolite, U.S.A.	6540.67	0.178		
	*	*		
$MnSiO_3$	6540.30	0.037	6540.69	0.081
Rhodonite, Australia	6541.03	0.043		
	*	*		
$NaMn_2Si_3O_8(OH)$	6540.29	0.040	6540.70	0.094
Serandite, Canada	6541.00	0.054		
	*	*		
α-Mn_2SiO_4	6540.20	0.037	6540.65	0.091
Tephroite olivine, France	6540.96	0.053		
	*	*		
MnO	6540.16	0.036	6540.62	0.073
Manganosite, synthetic	6541.06	0.038		
	*	*		
$MnCO_3$	6540.26	0.050	6540.65	0.091
Rhodocrosite, Argentina	6541.12	0.043		
	*	*		
$Mn_3Al_2Si_3O_{12}$	6540.20	0.019	6540.66	0.062
Spessartine garnet, Norway	6540.85	0.043		
	*	*		

transitions were computed as well, in order to better simulate the pre-edge feature (MULTIPOLE 2 0), which is a recently introduced important feature of FEFF8.2. Crystal structures for the models were taken from the literature, as described now.

B. Model compounds

Mn-bearing model compounds include a variety of oxides and silicates, natural or synthetic, and well characterized to contain manganese (redox states of II, III, and IV) in octahedral, cubic, or tetrahedral geometry. Tables I–III list the respective crystalline model compounds used in this study for Mn(II), Mn(III), and Mn(IV). Manganosite[1] (MnO, from Alfa Inc. and packaged in argon) did not show any evidence of surface oxidation. Other Mn(II)-bearing compounds include a carbonate ($MnCO_3$),[37] an olivine (α-Mn_2SiO_4),[38] a garnet ($Mn_3Al_2Si_3O_{12}$),[39] a pyroxenoid ($MnSiO_3$),[40] two hydrated silicates ($NaMn_2[Si_3O_8(OH)]$ and $(Fe,Mn)_2Al_9O_7(OH)[SiO_4]_4$),[41,42] as well as two synthetic Mn-bearing simple oxides (jacobsite spinel and maganonichromite).[43,44] Mn(III)-bearing models include the three modifications of MnOOH (α, β, and γ, respectively; the first two being synthetic).[45] Three other oxides were studied: Mn_2O_3,[46] $Zn_2Mn_4O_8$-H_2O, and $CaMn_2O_4$.[47] Finally, two networked Mn(III)-bearing structures were studied: a borocarbonate ($Ca_4Mn_3O_3[BO_3]_3[CO_3]$) and a phosphate ($MnPO_4$).[48,49] Mn(IV) models are all oxides: the three polymorphs of MnO_2 (α, β, and ϵ)[1,14] three hollandite-related structures [hollandite, cryptomelane, and cesarolite, respectively; generic formula $(Ba,K,Pb)Mn_8O_{16}$],[50] two end members of the romanechite-todorokite series ($\sim Ba_2Mn_5O_{10}$ and $CaMn_3O_7$-H_2O; the first containing 1/4 of its Mn as trivalent),[51] and two phyllomanganates ["chalcophanite" $ZnMn_3O_7$-$3H_2O$, and "lithiophorite" $LiAl_2Mn_3O_6(OH)_6$, respectively; these samples containing $\sim$25 at. % of Mn(III)].[52,53] Because of their chemical complexity, the last seven samples were extensively characterized by several methods prior to beam time, such as x-ray diffraction, proton-particle-induced x-ray emission, or transmission electron microscopy (TEM),[54] as well as the electron

TABLE II. Pre-edge information for the models for Mn(III). The asterisk indicates convergence to a null integrated area.

	Pseudo-Voigt function			
Sample	Energy (eV)	Integrated area	Centroid (eV)	Total integrated area
Mn_2O_3	6540.25	0.034	6540.91	0.094
Bixbyite, synthetic	6540.92	0.044		
	6542.37	0.012		
$Zn_2Mn_4O_8$—H_2O	6540.26	0.016	6541.04	0.078
Hydrohetearolite, U.S.A.	6540.97	0.0340		
	6541.74	0.022		
$CaMn_2O_4$	6540.47	0.040	6540.83	0.094
Marokite, Morocco	6541.17	0.041		
	*	*		
β-MnOOH	6540.38	0.052	6540.98	0.089
Feitknechtite, synthetic	6541.23	0.020		
	6542.65	0.016		
α-MnOOH	6540.88	0.036	6541.07	0.062
Groutite, synthetic	6541.34	0.025		
	*	*		
γ-MnOOH	6540.39	0.055	6541.03	0.086
Manganite, Germany	6541.23	0.012		
	6542.88	0.018		
$Ca_4Mn_3O_3(BO_3)_3CO_3$	6539.64	0.097	6540.76	0.093
Gaudefroyite, Namibia[a]	6541.02	0.023		
	6541.96	0.014		
$MnPO_4$	6540.12	0.019	6541.01	0.067
Purpurite, Namibia	6541.37	0.048		
	*	*		

[a]This sample might have some hausmanite inclusions, explaining its relatively low centroid position for Mn(III).

microprobe[55] (using the CAMPARIS facility at Université de Paris 6). Their structural formulas[25] are consistent with dominant amounts (e.g., >90 at. %) of tetravalent manganese, except for the lithiophorites [showing up to 30 mol % Mn(III)].

C. Experimental XANES methods

Mn *K* edge XANES spectra for these model compounds were collected at SSRL (Stanford, CA, U.S.A.) using the SPEAR3 storage ring. XANES data were collected on beamline 11-2 under high-resolution conditions by the use of a Si(220) double-crystal monochromator and 0.3 vertical height for the slits before and after the monochromator. The energy reproducibility of the monochromator was below 0.03 eV after 2 days of data collection. Pre-edge features were collected using 0.1 eV steps, whereas the main edge crest was collected with 0.3 eV steps to 300 eV above the absorption edge. The XANES spectra were normalized using a series of degree-3 polynomials, whose parameters were refined iteratively until the final spectrum was normalized (on the average) between 0 (before the edge) and 1 (after the edge). Then, the pre-edge region was extracted from the normalized XANES spectra and modeled using a series of pseudo-Voigt functions, as they require much less CPU time than true Voigt functions. To minimize the number of variable parameters, all pseudo-Voigt functions were modeled with a fixed width and Gaussian percentage. For the experiments presented here, the experimental resolution is ~1.3 eV (on beamline 11-2 at SSRL) and the core-hole lifetime of the Mn *K* edge is 1.1 eV.[56] A true Voigt function (with Gaussian experimental width and Lorentzian core-hole

TABLE III. Pre-edge information for the models for Mn(IV). The asterisk indicates convergence to a null integrated area.

Sample	Pseudo-Voigt function		Centroid (eV)	Total integrated area
	Energy (eV)	Integrated area		
$ZnMn_3O_7—3H_2O$[a]	6540.37	0.010	6541.37	0.0934
Chalcophanite, Mexico	6541.36	0.074		
	6542.43	0.010		
$\sim LiAl_2Mn_2O_6(OH)_6$[a]	6540.61	0.009	6541.37	0.0876
Lithiophorite, South Africa	6541.29	0.057		
	6541.91	0.021		
$CaMn_3O_7—H_2O$	6540.77	0.013	6541.55	0.0992
Todorokite, U.S.A.	6541.38	0.060		
	6542.35	0.026		
$PbH_2Mn_3O_8$	6540.73	0.010	6541.47	0.0803
Cesarolite, Tunisia	6541.30	0.054		
	6542.51	0.016		
$\sim BaMn_6Fe_2O_{16}$	6540.36	0.059	6541.57	0.0702
Hollandite, India	*	*		
	6542.69	0.011		
$\sim KMn_8O_{16}$	6540.59	0.013	6541.55	0.1614
Cryptomelane, Australia	6541.36	0.113		
	6542.52	0.035		
$\sim Ba_2Mn_5O_{10}$[a]	6540.43	0.008	6541.29	0.0775
Romanechite, France	6541.20	0.055		
	6542.11	0.014		
ϵ-MnO_2	6540.94	0.0299	6541.63	0.1126
Akhtenskite, Russia	*	*		
	6541.87	0.0827		
α-MnO_2	*	*	6541.59	0.0737
Ramsdellite, U.S.A.	6541.26	0.0593		
	6542.95	0.0144		
β-MnO_2	*	*	6541.45	0.0776
Pyrolusite, Mexico	6541.25	0.0635		
	6542.35	0.0140		

[a]This sample also contains some minor amounts of Mn(III).

lifetime) was calculated to be equivalent (at the 99.9% confidence level) to a pseudo-Voigt function with a 1.4 eV width and a Gaussian percentage of 45%. These two parameters were consequently fixed in the fitting of the pre-edge region presented in this study. However, a continuum of 2–4 pseudo-Voigt functions was allowed to freely vary to account for the baseline (as the sum of these pseudo-Voigt functions). This method was validated at the Fe *K* edge through comparative Fe *K* edge RIXS and XANES experiments for a series of models.[55,57,58] Tables I–IV report the pre-edge data for the samples of this study, which include the individual positions and integrated areas for each significant pseudo-Voigt function. The pre-edge information for each sample (centroid and total integrated area) is calculated (1) from the

TABLE IV. Pre-edge information for the complex oxides.

Sample	Pseudo-Voigt function		Centroid (eV)	Total integrated area
	Energy (eV)	Integrated area		
Mn_3O_4	6540.02	0.013	6540.89	0.174
Hausmannite	6540.69	0.131		
	6542.11	0.030		
Mn_7SiO_{12}	6541.10	0.049	6541.65	0.130
Braunite	6541.55	0.047		
	6542.59	0.034		
γ-MnO_2	6540.39	0.017	6541.32	0.129
N'sutite	6541.27	0.090		
	6542.26	0.022		
$NaMn_7O_{14}$—$1.3H_2O$	6540.76	0.038	6541.61	0.084
Birnessite-Na	6541.55	0.022		
	6543.05	0.023		

average position of the pseudo-Voigt functions, weighted by their respective integrated areas, and (2) from the sum of the individual integrated areas.

III. RESULTS

Tables I–III present the results of the pre-edge models for model compounds containing divalent, trivalent, and tetravalent manganese. Three pseudo-Voigt functions were systematically considered for the model of the pre-edge features *sensu stricto*. For some compounds, a pseudo-Voigt function converged to a null height (and, if occurring, was then excluded from the model). Figures 2, 4, and 6 show the experimental information collected for Mn(II), Mn(III), and Mn(IV), respectively. Figures 3, 5, and 7 show the FEFF8.2 calculations performed on selected structural configurations containing these redox states.

A. Divalent manganese

The pre-edge feature for centrosymmetric sites around Mn(II) (O_h as in $MnCO_3$ and MnO, for instance) shows a well-resolved doublet [Figs. 2(a) and 2(b)]. Polarized resonant inelastic x-ray scattering experiments performed at the Mn *K* edge in a single crystal of MnO also evidenced a doublet, which was assigned to the transition of the 1*s* electron to the 3*d* crystal-field-split states (t_{2g} and e_g, respectively),[31] in agreement with powder (i.e., anisotropic)

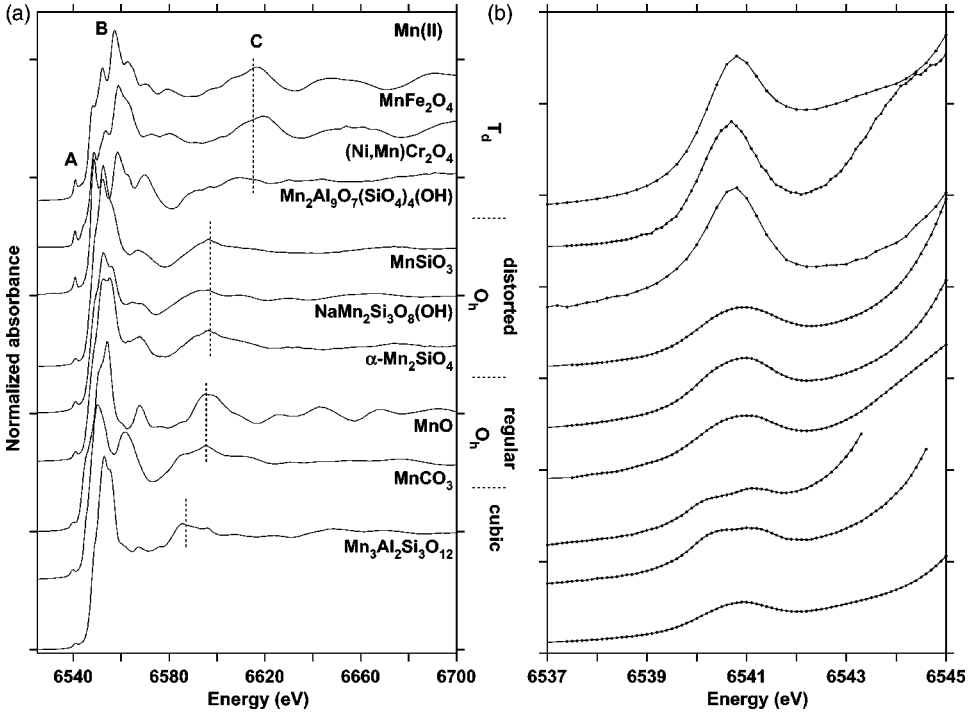

FIG. 2. Mn *K* edge normalized XANES spectra for the Mn(II)-bearing model compounds investigated in this study containing Mn(II) in tetrahedral, octahedral (centrosymmetric and distorted), and cubic sites: (a) main XANES spectra; (b) detail of the pre-edge region.

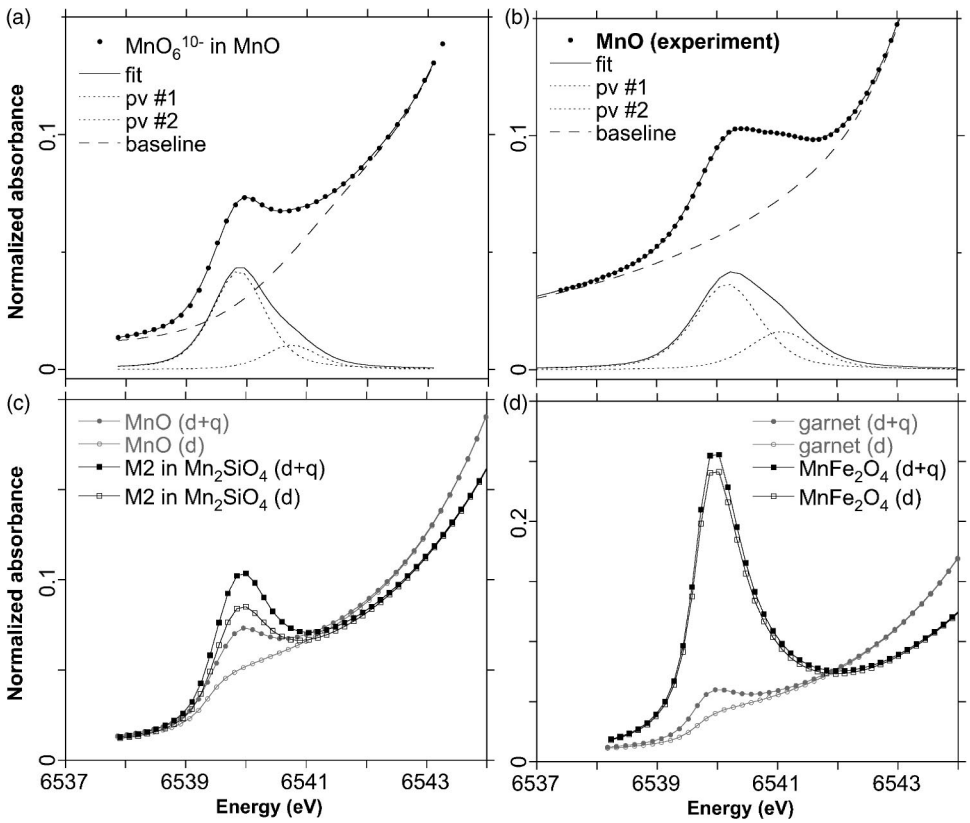

FIG. 3. *Ab initio* FEFF8.2 calculations for Mn(II)-bearing structures: (a) model of the O_h site (as in MnO) and its model, showing the two pseudo-Voigt functions that are required to fit the simulation; (b) model of the experimental spectrum; (c) variation in pre-edge shape as a function of transition type (dipolar *d* and/or quadrupolar *q*) for Mn(II) in regular and distorted octahedral sites (as in MnO and the *M*2 sites of α-Mn_2SiO_4); (d) same as (c) but in cubic (as in garnet) and tetrahedral (as in spinel) sites.

RIXS experiments.[21] The pre-edge feature becomes broadened for more octahedrally distorted Mn sites (as in $MnSiO_3$ or α-Mn_2SiO_4 for instance). A doublet is also observed for Mn(II) in the centrosymmetric cubic site of garnet. When under T_d symmetry, the pre-edge appears as a singlet, with a higher height ($\sim$2 as compared to O_h), as observed for many other transition elements.[58–60] However, two pseudo-Voigt functions are still required to model this feature (see Table I bottom).

Ab initio FEFF8.2 calculations of the pre-edge region[1] of MnO were then conducted to better understand the origin of this feature. There is a good agreement between FEFF8.2 pre-edge calculations [Fig. 3(a)] and the experiment [MnO; Fig. 3(b)]. The pre-edge feature appears when the first oxygen neighbors and quadrupolar transitions are accounted for [Fig. 3(c)]. This indicates that the origin of this feature is not related to distant neighbor shells,[27] but rather comes from the classical *p-d* hybridization model involving dipolar and quadrupolar transitions among the crystal-field-split states related to oxygen first-neighbor ligands. An indirect validation of this model is that the pre-edge features for rhodocrosite ($MnCO_3$) and manganosite (MnO) are nearly identical in shape, intensity, and position [Fig. 1(c)], although the $Mn(II)O_6^{10-}$ moieties contained in these three structures are surrounded by very different atoms at very different distances.[1,37] Mutiplet calculations performed on Mn(II) in O_h symmetry (as in MnO) report two groups of transitions.[21] One-electron calculations cannot calculate discrete electronic transitions as multiplets do, so each set of transitions was "simulated" by FEFF8.2 as a broadened interference, which was then modeled as pseudo-Voigt functions [Fig. 3(a)]. Therefore, the agreement between multiplet calculations and FEFF8.2 is excellent.

From the present database of model compounds, additional information can be obtained. For instance, when the site distortion increases (from $MnCO_3$ to $MnSiO_3$), the contribution of dipolar transitions increases accordingly; hence the higher integrated pre-edge intensity ($0.073 \rightarrow 0.094$; Table I). FEFF8.2 confirms these evolutions, as suggested by the greater pre-edge intensity when Mn(II) is located in the highly distorted *M*2 site of α-Mn_2SiO_4 (an olivine structure) [Fig. 3(c)]. As for other transition metals, pre-edge areas are not a measurement of coordination (as often reported) but of symmetry, as suggested by the similar pre-edge information for garnet[39] (cubic symmetry, eight coordinated) and manganosite[1] (octahedral, six coordinated). FEFF8.2 calculations confirm that the pre-edge for Mn(II) in the cubic site of garnet has a relatively low intensity, typical of centrosymmetric sites [Fig. 3(d)] for which quadrupolar transitions dominate over dipolar ones (as for the octahedral symmetry). Finally, the most intense pre-edges are calculated for the tetrahedral (T_d) geometries [as in $MnFe_2O_4$; Fig. 3(d)]. However, as predicted for noncentrosymetric sites, the dipolar contribution to the pre-edge dominates highly over the quadrupolar one under T_d geometry. Thus there is excellent agreement between experiment and the *ab initio* FEFF8.2 simulations for a variety of symmetries around Mn(II), provided that quadrupolar transitions are accounted for.

B. Trivalent manganese

The pre-edge region for Mn(III)-bearing models shows a doublet [Figs. 4(a) and 4(b)], the second feature being located at 2 eV from the first one. However, three pseudo-

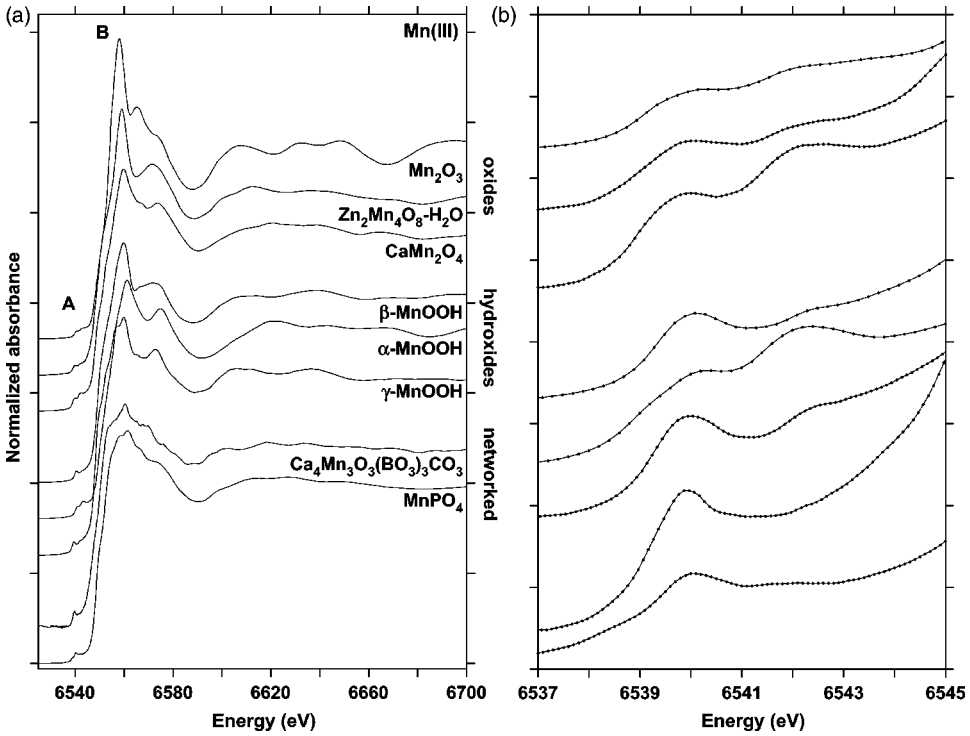

FIG. 4. (a) Mn *K* edge normalized XANES spectra for the Mn(III)-bearing model compounds investigated in this study (either oxides, hydroxides, or networked); (b) detail of the pre-edge region.

Voigt functions were required to properly model this pre-edge (Table III). The second pseudo-Voigt function is not clearly visible in most pre-edges, but its presence significantly improved the model [Fig. 5(a)]. The second feature of the doublet (i.e., the third pseudo-Voigt function in the model) has a highly variable height among the samples, from nearly invisible in gaudefroyite to very intense in α-MnOOH (groutite) or $CaMn_2O_4$ (marokite). The local structure around Mn in the last compound is more radially distorted than in gaudefroyite [their respective variance in the O—Mn—O angles inside the $Mn(III)O_6$ polyhedra is 1145 versus 1034 deg^2].[45,48] Hence, as for Mn(II), there is a direct relationship between the height or area of this pre-edge feature and the Mn-site centrosymmetry. No samples containing tet-

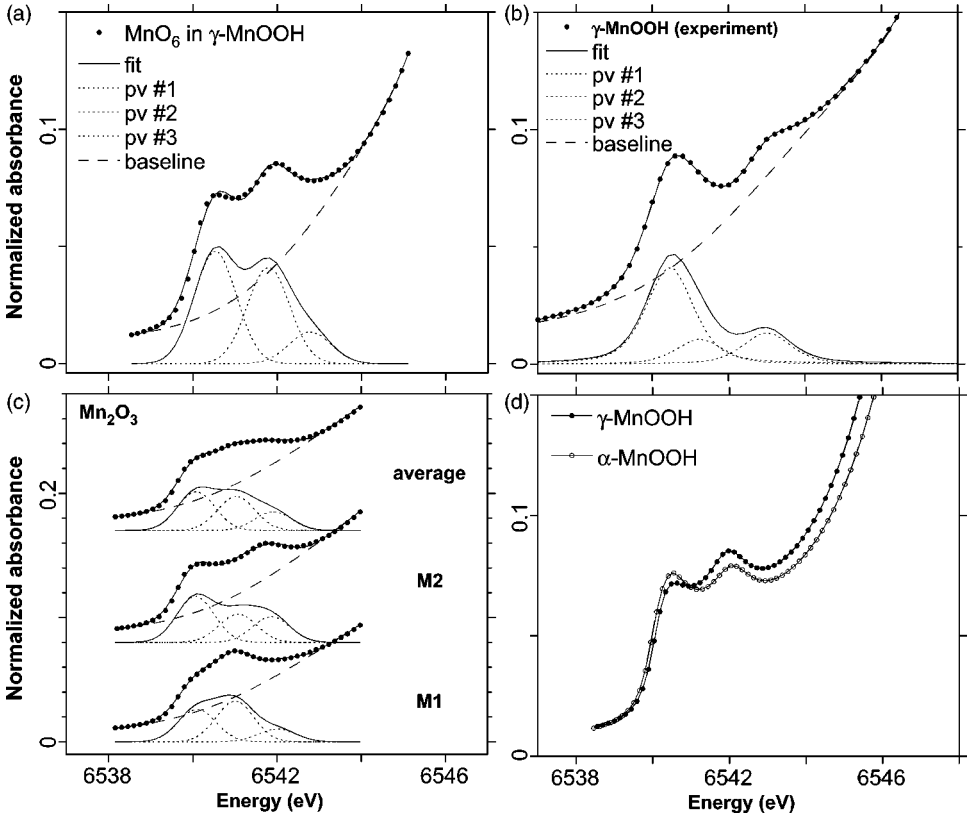

FIG. 5. *Ab initio* FEFF8.2 calculations for Mn(III)-bearing structures: (a) model of the FEFF8.2 simulation for β-MnOOH, showing the three pseudo-Voigt functions required to fit the simulation; (b) equivalent of (a) for the experimental spectrum; (c) influence of site centrosymmetry as in Mn_2O_3, in which two sites exists, a regular (*M*1) and a Jahn-Teller-distorted (*M*2) site and the average of both (shown with their best fit); (d) study of the Jahn-Teller distortion in two modifications of MnOOH.

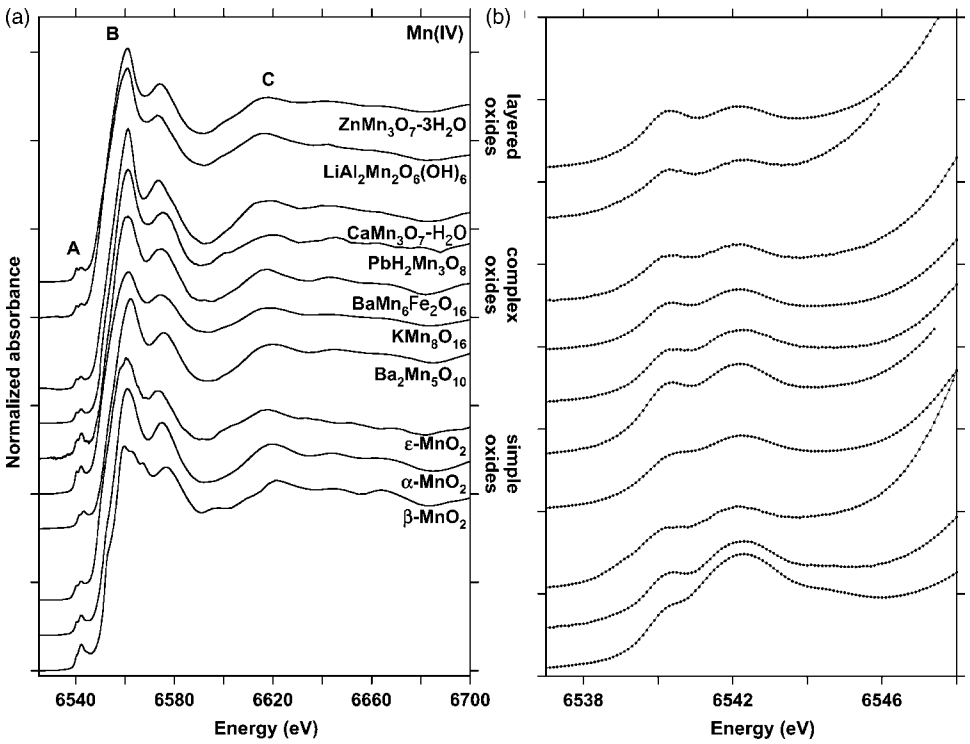

FIG. 6. (a) Mn *K* edge normalized XANES spectra for the Mn(IV)-bearing model compounds investigated in this study (either layered hydroxides, complex oxides, or simple oxides); (b) detail of the pre-edge region.

rahedrally coordinated Mn(III) could be studied as the great majority of the compounds containing trivalent manganese show octahedrally coordinated Mn(III).

Around Mn(III) (as in manganite),[45] three main sets of transitions are predicted by FEFF8.2 [Fig. 5(a)] and measured in manganite [Fig. 5(b)]. These transitions closely resemble those for Fe(II) in O_h symmetry for which 2+1 sets of transitions were also predicted and measured.[21,28,55] On the other hand, multiplet calculations evidenced a continuum of transitions, which can be grouped into five major sets of transitions.[21] The last group of transitions (near 6548 eV) is too weak in intensity, so it could not be observed using FEFF8.2, due to broadening effects inherent in the use of a one-electron theory (like FEFF8.2). However, given its relative area,[21] the influence of that set of transitions should be negligible on the pre-edge information. The second to fourth sets of transitions (between 6543.5 and 6545.5 eV) are too close to each other[21] to be resolved by XANES methods (as for Fe).[60] They can be best modeled by two transitions (unfortunately physically nonrealistic but statistically meaningful). Then, there is good agreement between FEFF8.2 and multiplet theory results about the transition energies. In contrast, the agreement between FEFF8.2 and the multiplet results is less good for the predicted intensities for each group of transitions. For instance, according to FEFF8.2, the first set of transitions should be the most intense in β-MnOOH, whereas it is the second for the multiplet calculations (and vice versa). However, most compounds containing Mn(III) show a severe Jahn-Teller effect,[45] which distorts strongly the $Mn(III)O_6^{9-}$ moieties, making such features not easily computable using multiplets, and the comparison with FEFF8.2 is inaccurate.

To better comprehend these Jahn-Teller-related effects on the pre-edge for Mn(III), the two sites present in Mn_2O_3 [Fig. 5(c)] were studied. In this bixbyite structure, trivalent manganese is distributed over a centrosymmetric $M1$ site and a highly distorted (Jahn-Teller-distorted) $M2$ site.[46] In the $M1$ site (in which no Jahn-Teller distortion occurs), the first set of transitions (near 6540 eV) has a lower relative intensity as compared to the second set of transitions (near 6541 eV). Then the agreement between FEFF8.2 and multiplet results is excellent. When Jahn-Teller distortion occurs (as in the $M2$ site), the relative intensities of these two sets of transitions are reversed. The $M1$-$M2$ averaged pre-edge feature was computed and modeled [top curves in Fig. 5(c)]. The two first sets of transitions show therefore comparable areas. Identical conclusions can be reached from the study of other Mn(III)-bearing oxides, hydroxides, and carbonates that were investigated (such as marokite, groutite, feitknechtite, purpurite, gaudefroyite, etc.) for which the intensity of the second set of transitions varies quite significantly as a function of site distortion [within the already Jahn-Teller-distorted sites; see Fig. 4(d) in which the α and β modifications of MnOOH are compared].

C. Tetravalent manganese

As for Mn(III), most compounds containing tetravalent manganese have this cation in octahedral sites, as suggested by the relatively low pre-edge heights for these compounds (Table III). The pre-edge feature usually shows a doublet [Figs. 6(a) and 6(b)] for which the second feature has a highly variable height among the compounds. A third feature is also observed near 6545 eV in the most ordered oxides, such a α- and β-MnO_2. On the other hand, the XANES spectra for most of these models look relatively similar to each other (with the exception of β-MnO_2).

FEFF8.2 calculations for pre-edge feature for the $Mn(IV)O_6^{8-}$ moieties (as in β-MnO_2 pyrolusite) [Fig. 7(a)]

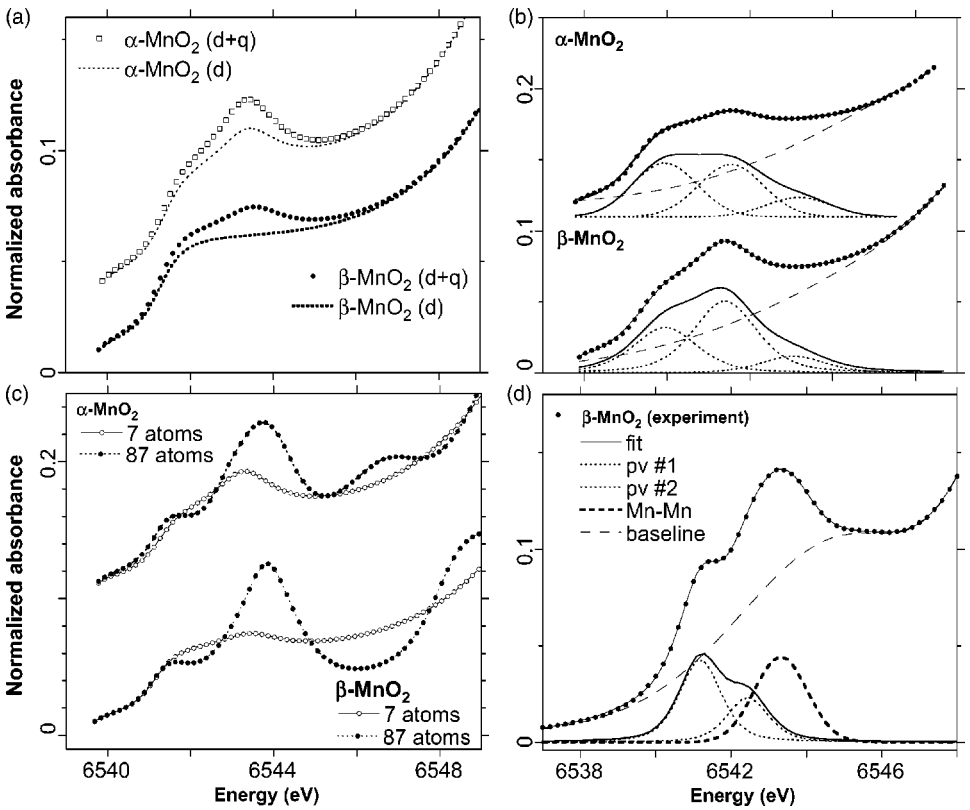

FIG. 7. *Ab initio* FEFF8.2 calculations for Mn(IV)-bearing structures: (a) model of the O_h symmetry in the α- and β- modifications of MnO_2, showing the importance of quadrupolar transitions and centrosymmetry on the pre-edge intensity; (b) best fits calculated for these two modifications, evidencing the need for three pseudo-Voigt functions to model the pre-edge and their respective variation as a function of distortion; (c) influence of distant manganese neighbors on the pre-edge feature of β-MnO_2; (d) typical model of the experiment for Mn(IV) in which two or three pseudo-Voigt functions are required to model the pre-edge *sensu stricto*, whereas an additional pseudo-Voigt function is needed for the metal-metal transitions.

shows two distinct features, provided quadrupolar transitions are accounted for. Multiplet calculations for a Mn(IV) ion in O_h symmetry[21] agree with the FEFF8.2 predictions for the $Mn(IV)O_6^{8-}$ moiety in β-MnO_2 [Fig. 7(a)]. The multiplet theory suggests that four main sets of transitions are predicted for such Mn(IV), which can be rationalized to three main sets of transitions using the one-electron theory of FEFF8.2 [Fig. 7(b)]. A third pseudo-Voigt function of very low intensity [located near 6545 eV; Fig. 6(b)] is required in the model as it contributes to the pre-edge asymmetry. As for Mn(II) and Mn(III), the intensity of the second pre-edge feature (near 6543 eV) is found to increase with site distortion, as shown on Fig. 7(a) for the α and β modifications of MnO_2.

However, the highly resolved doublet observed experimentally [see Fig. 6(b)] is not reproduced using these models. Similar inconsistencies for Mn(IV) were also reported for pre-edges extracted from Mn *K* edge XANES and RIXS experiments in organometallic systems.[21] The discrepancies are attributed to variations in the effective number of 3*d* electrons, more importantly for Mn(IV) than for Mn(II), the latter exhibiting an almost pure $1s3d$ excited-state configuration.[21] However, for Mn(V), Mn(VI), and Mn(VII), no such discrepancies are observed in their pre-edge feature among the models studied.[54] Alternatively, the possibility of metal-metal transitions should also be investigated, as they are known to produce extra transitions in the pre-edge region of many other 3*d* transition elements, particularly in highly polymerized oxides such as TiO_2, FeO, Fe_2O_3, Fe_3O_4, and NiO.[29,33,34]

Accordingly, 12–20 Mn next-nearest neighbors are located near 5.2–5.3 Å around the central Mn in the three modifications of MnO_2 studied here. Only when these neighbors are considered does the calculated pre-edge spectrum match the experiment nearly ideally [Fig. 7(c)]. However, the second and third pseudo-Voigt functions arising from crystal-field splitting (near 6543 and 6545 eV) overlap strongly with the transition related to metal-metal pairs [Fig. 7(c)]. Consequently, these transitions cannot be separated in the experiment, even under high-resolution conditions. Therefore, the pre-edge for Mn(IV) is complex and must be modeled with great caution. The most robust approximation was achieved by considering four pseudo-Voigt functions for the pre-edge of Mn(IV): three for the pre-edge *sensu stricto* [which can degenerate into two pseudo-Voigt functions in some cases, as in β-MnO_2; see Fig. 7(d)] and a last one for the metal-metal transitions [Fig. 7(d)]. However, this last "metal-metal" pseudo-Voigt function in the model of the experiment (near 6545 eV) still contains much information related to the pre-edge *sensu stricto* [according to Fig. 7(a)]. The nonconsideration of this information for the estimation of redox state and symmetry around Mn(IV) is estimated, thanks to Fig. 7(c), to be less than 10%, which is the accuracy of the method. Worse, the second pseudo-Voigt function modeled for the experimental pre-edge spectrum for β-MnO_2 is significantly underestimated according to the FEFF8.2 model presented on Fig. 7(b). This last figure suggests that, in this compound, the second pseudo-Voigt function has a greater intensity than its lower-energy counterpart, in contrast to the model of the experiment [Fig. 7(d)]. At this point, the energy resolution of the current XANES experiments at the Mn *K* edge is not enough to separate each of these contributions and, therefore, limits drastically the extraction of reliable pre-edge information for Mn(IV). However, the model presented above re-

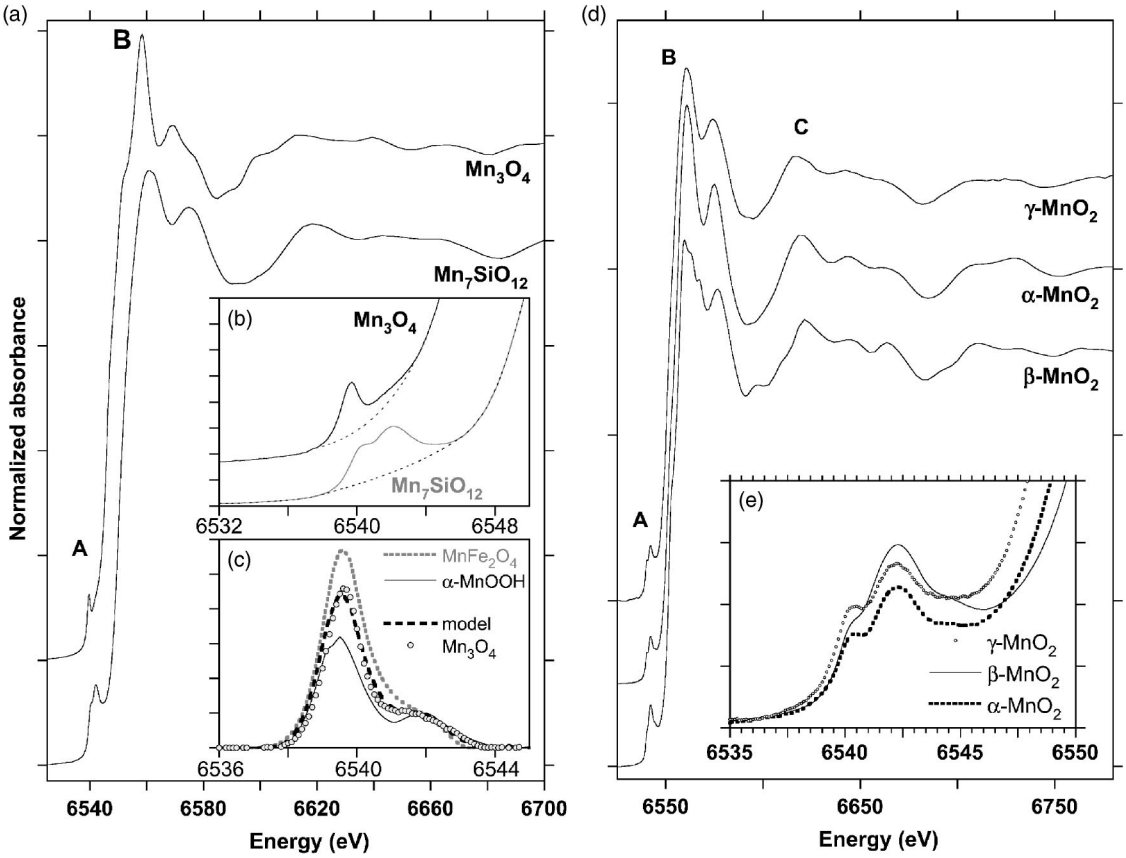

FIG. 8. Normalized Mn *K* edge XANES and pre-edge spectra for multivalent manganese oxides: (a) normalized Mn *K* edge XANES for Mn_3O_4 and Mn_7SiO_{12}; (b) detail of the respective pre-edges for Mn_3O_4 and Mn_7SiO_{12}; (c) model of the pre-edge for Mn_3O_4 considering that for spinel and α-MnOOH; (d) normalized Mn *K* edge XANES and pre-edge spectra for and γ-MnO_2 spectra as compared to α- and β-MnO_2; (e) detail of the pre-edge region.

mains correct in the absence of more oxidized redox states of manganese, such as V, VI, or VII. In all cases, the model for Mn(IV) must be used with great care and wisely.

IV. DISCUSSION

A. Summary for model compounds

The pre-edge centroids for the 2+, 3+, and 4+ oxidation states of manganese shift consistently toward higher energy with higher oxidation state. They are centered around 6540.65, 6541.00, and 6541.55(5) eV, respectively (with standard deviations of 0.03–0.05 eV). The standard deviation in the centroid position for a given redox state of manganese corresponds to a 5–15 % in accuracy for a redox determination (average ~10%). This error in redox determination is considerably lower than that for the edge measurements (25–90 %; average ~40%).

As for other transition elements,[58–60] the pre-edge areas increase with site distortion but also with redox state (as more empty 3*d* levels are created by the ionization of Mn). *Ab initio* calculations, assuming the one-electron theory of FEFF8.2, are in good agreement with multiplet calculations,[21] provided that quadrupolar transitions are accounted for. However, the consideration of metal-metal transitions is critical, particularly in Mn(IV)-dominant samples [which can be qualitatively inferred from the edge position as shown on Fig. 1(b)]. This explains why previous attempts to extract reliable redox information from the Mn *K* edge pre-edge feature were unsuccessful.[20] Similarly, metal-metal transitions were previously reported for the rutile modification of TiO_2 (at the Ti *K* edge), FeO, Fe_2O_3 (at the Fe *K* edge), or NiO (at the Ni *K* edge).[29,30,33,34] However, when Mn(IV) in not polymerized [as shown for Mn(IV) in the acetylacetonate],[21] these metal-metal transitions disappear, making the model of the pre-edge more robust. In the following examples, the above models are applied to a variety of samples of physical interest and discussed in the light of the literature.

B. Application to complex manganese oxides

1. Multivalent oxides

In Mn_3O_4, Mn is distributed over two sites and two redox states [$^{[4]}$Mn(II) and $^{[6]}$Mn(II)].[3] Accordingly, the pre-edge centroid is located near 6540.89 eV, in between the domains for Mn(III) and Mn(II) [see Table IV; Figs. 1(b) and 8(a)–8(c)]. Also, the relatively high pre-edge area (0.174) is related to the presence of the tetrahedrally coordinated Mn(II). A computed mixture between $MnFe_2O_4$ and α-MnOOH model compounds [see Fig. 8(c)] confirms that a 50:50 me-

chanical mixture between both models has a centroid located at 6540.85(5) eV, which is halfway (as predictable) between that for Mn(II) and that for Mn(III) (6540.65 and 6541.00 eV, respectively). However, the pre-edge height for Mn_3O_4 is not halfway but ~80% of that for a T_d geometry around Mn(II) (their total integrated areas are even closer). Such nonlinearities in the pre-edge information variation for mixtures of redox states and coordination environments were suspected as they were previously shown for iron.[55]

These predictions[55] also suggest that, when the redox state varies at a constant geometry (as in Mn_7SiO_{12} or "braunite,"[61] see Fig. 6 and Table IV), the pre-edge information varies linearly as a function of redox (i.e., the pre-edge centroid varies at a constant pre-edge area). In Mn_7SiO_{12}, the pre-edge centroid (6541.65 eV) suggests the presence of dominant amounts of Mn(IV) with no detectable amounts of Mn(III). A stoichiometric analysis of that sample shows that 7 mol % of the total manganese is trivalent (confirming indirectly that the sensitivity of the XANES method presented here is 10 mol %). Similarly, the redox state of manganese can be estimated in the γ- modification of MnO_2 [see Fig. 8(d)], which is an important cathodic material in dry-cell batteries. This material was shown, thanks to transmission electron microscopy, to be a complex mixture of the α and β modifications of MnO_2, together with highly defective domains and tunnels, in which a variety of cations (such as alkali and alkaline-earth metals) and water molecules occur, which should stabilize in turn some Mn(III).[62] The Mn *K* edge XANES of γ-MnO_2 [Fig. 8(d)] shows broad features (as in α-MnO_2). This suggests that the β-MnO_2 type of domain does not predominate in that sample [because they promote highly structured XANES signatures, in contrast to α -MnO_2 which XANES is broader; see Fig. 8(d)]. From linear combinations of the end members shown in Fig. 8(d), the relative amount of β-MnO_2 is less than 1/4 in volume in that sample. Using electron microprobe and stoichiometric considerations, the amount of Mn(III) (in aperiodic, defective domains[62]) in this γ-MnO_2 is ~20 mol %. The measured fraction of trivalent manganese by the pre-edge method [0.40(5)] is much higher. Despite this mediocre agreement, the direct XANES measurement are recommended over stoichiometric estimates, which strongly rely on an accurate measurement of the total oxygen content (including hydroxyls, which are always difficult to measure accurately).

2. Defective oxides

Defective manganese oxides, such as $NaMn_7O_{12}$-$1.3H_2O$ ("birnessite") are structurally and chemically complex phases, which are common as the result of low-temperature oxidation of more simple, high-temperature oxides.[2] Their exact structure is still debated, in part because of the presence of trivalent manganese, which balances various charge-compensating cations (such as Na) that can be accommodated in the tunnels of the host structure.[63–65] Therefore, an accurate measurement of the speciation of manganese in these compounds is essential to better understand their defective structure. In shape, the pre-edge for $NaMn_7O_{12}$ -$1.3H_2O$ is intriguingly similar to that for γ-MnOOH, but shifted by +0.58(3) eV. The pre-edge position for the defective oxide (6541.61 eV) is then consistent with the presence of dominant amounts of Mn(IV) with less than 10 mol % of Mn(II) and/or Mn(III). This direct measurement is in good agreement with indirect chemical information derived from structural formula,[64,65] which show that less than 1/3 of the manganese can be trivalent in these phases (together with some minor amount of divalent manganese).

Mn *K* edge XANES calculations were undertaken for $NaMn_7O_{12}$-$1.3H_2O$ (based on Ref. 64) to better understand the origins of the pre-edge feature in this defective structure. Self-consistency was forced to converge to reasonable values for the effective charge (e.g., −0.2 for oxygen, 0.1–0.2 for Na or Mg, and 0.35 for manganese), as the Na site favored anomalously low electronic densities, as refined. Also, an infinitively periodic structure was considered, which does not hold for the local vacancies and substitutions known in these networks.[64] Despite these limitations, the agreement within the XANES region with the experiment is fair (particularly features *B* and *C* in Fig. 9), despite the XANES intensities are overestimated (due to the fully periodic model used in FEFF8.2). The pre-edge-simulated feature (feature *A* in Fig. 9) reproduces well the measured doublet. However, the distant manganese neighbors located between 5 and 6 Å around the central absorbing manganese must be taken into account to reproduce the experiment [as for the polymorphs of Mn(IV)O_2]. This result apparently contradicts that obtained for γ-MnOOH [Fig. 5(a)]. In γ-Mn(III)OOH, a similar pre-edge feature was collected (but shifted by −0.58 eV because of the presence of Mn(III) instead of Mn(IV). However, no distant Mn next-nearest neighbors were required to model the pre-edge feature of that manganite, in contrast to $NaMn_7O_{12}$-$1.3H_2O$.

Consequently, the shape of the pre-edge alone should not be used as an indicator of the speciation of Mn (either redox or environment). Instead, the pre-edge centroid information must be evaluated first, in order to derive the amount of Mn(IV) in the structure. If the pre-edge centroid is found close to that for Mn(IV) oxides, the possibility for Mn—Mn pairs in the pre-edge must be considered, particularly when the polymerization of Mn(IV) is high (as in Mn oxides and hydroxides such as phyllomanganates). In turn, the pre-edge region for Mn(IV)-bearing compounds is a measure of the polymerization of Mn moieties at distances above 5 Å, the latter neighbors appearing less important contributors through conventional EXAFS spectroscopy.[5,65] A direct consequence for most Mn(IV)-rich compounds is that the prediction of their pre-edge feature is impossible if the structure is unknown (such as when the structure is defective or amorphous). Also, from the experimental information, it is likely that the centroid for the triplet of pseudo-Voigt functions (used to model the pre-edge) is somewhat overestimated because of the presence of Mn—Mn pairs. In $NaMn_7O_{12}$ -$1.3H_2O$, that centroid is actually centered at 6541.61 eV, which is +0.06 eV above the average value for Mn(IV) [based on the database of Mn(IV)-bearing model compounds investigated in this study]. Consequently, one could overestimate (~+10%) the actual Mn redox state in this compound. This last example highlights a limitation of the method in the case of Mn(IV)-rich compounds (when structural and/or ultra-high-resolution spectroscopic—e.g.,

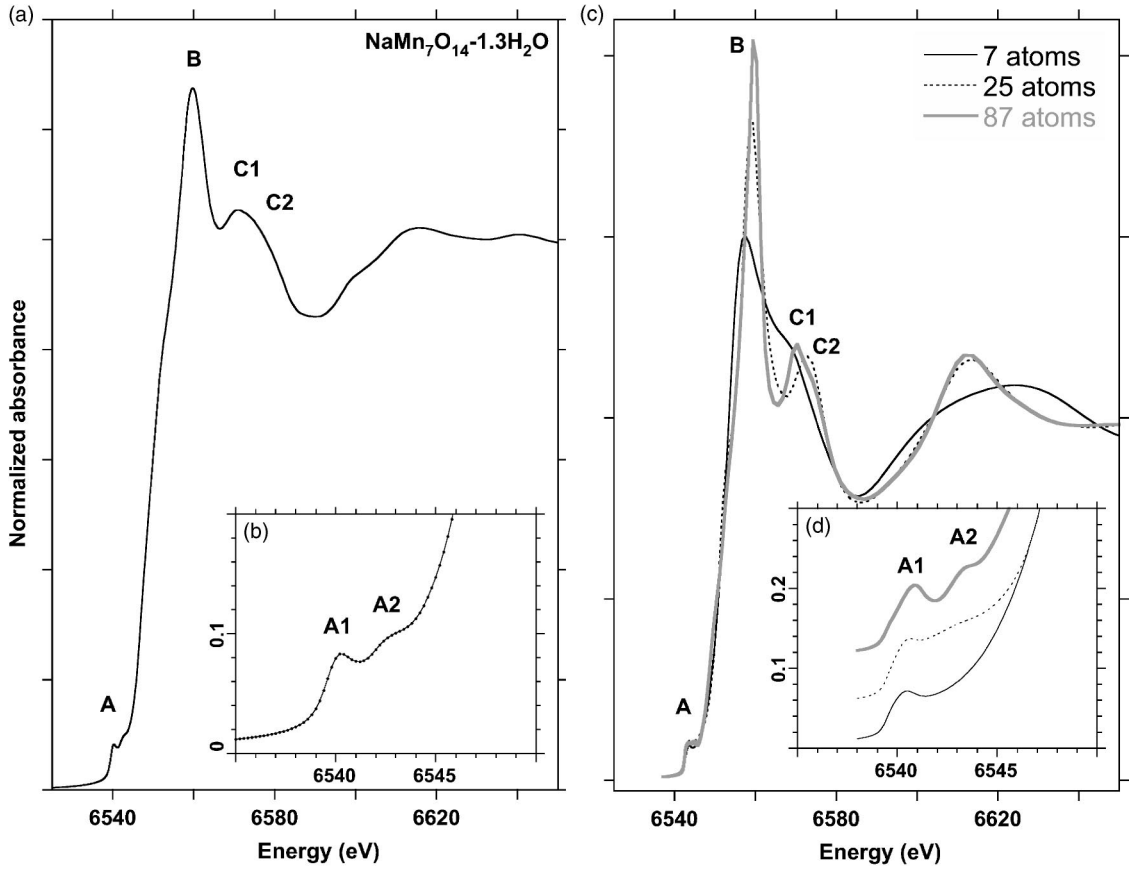

FIG. 9. Normalized Mn *K* edge XANES and pre-edge spectra (insets) for defective $NaMn_7O_{14}$-$1.3H_2O$: (a), (b) experiment; (c), (d) *ab initio* FEFF8.2 models.

RIXS—information is lacking). In any case, the pre-edge region of the Mn *K* edge XAFS spectra for manganese-oxide-type compounds still provides complementary information to the main XANES and EXAFS regions, but the pre-edge for Mn(IV)-bearing compounds must be analyzed with care.

C. Conclusions

Thanks to *ab initio* FEFF8.2 calculations, reliable redox and symmetry information can be extracted from the pre-edge region, provided that quadrupolar transitions are taken into account and that metal-metal pairs are excluded from the pre-edge feature models. In turn, these metal-metal transitions are useful indicators to estimate the degree of Mn(IV) ordering and polymerization. Further applications are under way to environmental and historical systems,[24,66] as well as for better understanding of the relation between the tunnel geometry in manganese oxides and the pre-edge features.

ACKNOWLEDGMENTS

The author wishes to thank Emilie Chalmin and John R. Rehr, who helped in the data reduction and interpretation. The staff of SSRL and ESRF (especially John R. Bargar, Gordon E. Brown, Jr., and Joe Rodgers) are warmly thanked for their help in every step of the data collection.

*Electronic mail: farges@univ-mlv.fr

[1] G. A. Waychunas, in *Oxide Minerals: Petrologic and Magnetic Significance*, edited by D. H. Lindsley, Reviews in Mineralogy Vol. 25 (Mineralogical Society of America, Washington, D.C., 1991).
[2] J. E. Post, Proc. Natl. Acad. Sci. U.S.A. **96**, 3447 (1999).
[3] V. Baron, J. Gutzmer, H. Rundlof, and R. Tellgren, Am. Mineral. **83**, 786 (1998).
[4] A. Manceau, A. Gorshkov, and V. Drits, Am. Mineral. **77**, 1133 (1992).
[5] A. Manceau, A. Gorshkov, and V. Drits, Am. Mineral. **77**, 1144 (1992).
[6] D. G. Schulze, S. R. Sutton, and S. Bajt, Soil Sci. Soc. Am. J. **59**, 1540 (1995).

[7] D. A. Mc Keown and J. E. Post, Am. Mineral. **86**, 701 (2001).
[8] C. A. Guest, D. G. Schulze, I. A. Thompson, and D. M. Huber, Soil Sci. Soc. Am. J. **66**, 1172 (2002).
[9] M. A. Marcus, A. Manceau, and M. Kersten, Geochim. Cosmochim. Acta **68**, 3125 (2004).
[10] D. G. Schulze, T. McCay-Buis, S. R. Sutton, and D. M. Huber, Phytopathology **85**, 990 (1995).
[11] K. W. Mandernack, J. Post, and B. M. Tebo, Geochim. Cosmochim. Acta **59**, 4393 (1995).
[12] J. R. Bargar, B. M. Tebo, and J. E. Villinski, Geochim. Cosmochim. Acta **64**, 16,2775 (2000).
[13] B. M. Tebo, J. R. Bargar, B. G. Clement, G. J. Dick, K. J. Murray, D. Parker, R. Verity, and S. M. Webb, Annu. Rev. Earth Planet Sci. **32**, 287 (2004).
[14] F. V. Chukhrov, A. I. Gorshkov, A. V. Sivtsov, V. V. Berezovskaya, YuP. Dikov, G. A. Dubinina, and N. N. Varinov, Int. Geol. Rev. **31**, 1068 (1989).
[15] N. Moelders, P. J. Schilling, J. Wong, J. W. Roos, and J. L. Smith, Environ. Sci. Technol. **35**, 3122 (2001); T. Ressler, J. Wong, J. Roos, and J. L. Smith, Environ. Sci. Technol. **34**, 950 (2000).
[16] D. A. McKeown, W. K. Kot, Hao Gan, and I. L. Pegg, J. Non-Cryst. Solids **328**, 71 (2003).
[17] K. K. Gunter, L. M. Miller, M. Aschner, R. Eliseev, D. Depuis, C. E. Gavin, and T. E. Gunter, Neurotoxicology **23**, 127 (2002).
[18] M. Belli, A. Scafati, A. Bianconi, S. Mobilio, L. Palladino, A. Reale, and E. Burattini, Solid State Commun. **35**, 355 (1980).
[19] R. Nietubyc, E. Sobczak, and K. E. Attenkofer, J. Alloys Compd. **328**, 126 (2001).
[20] H. Visser, E. Anxolabihhre-Mallart, U. Bergmann, P. Glatzel, J. H. Robblee, S. P. Cramer, J. Gìrard, K. Sauer, M. P. Klein, and V. K. Yachandra, J. Am. Chem. Soc. **123**, 7031 (2001).
[21] P. Glatzel, U. Bergmann, J. Yano, H. Visser, J. H. Robblee, W. Gu, F. de Groot, G. Christou, V. L. Pecoraro, S. P. Cramer, and V. K. Yachandra, J. Am. Chem. Soc. **136**, 9946 (2004).
[22] I. Reiche, C. Vignaud, B. Champagnon, G. Panczer, C. Brouder, G. Morin, A. Solé, L. Charlet, and M. Menu, Am. Mineral. **86**, 1519 (2001).
[23] S. Quartieri, M. Triscari, G. Sabatino, F. Boscherini, and A. Sani, Eur. J. Mineral. **14**, 749 (2002).
[24] F. Farges, E. Chalmin, C. Vignaud, I. Pallot-Frossard, J. Susini, J. Bargar, G. E. Brown Jr., and M. Menu, Phys. Scr. (to be published).
[25] E. Chalmin, F. Farges, J. Susini, J. R. Bargar, and G. E. Brown Jr., (unpublished).
[26] F. de Groot, Chem. Rev. (Washington, D.C.) **101**, 1779 (2001).
[27] B. Gilbert, B. H. Frazer, A. Belz, P. G. Conrad, K. H. Nealson, D. Haskel, J. C. Lang, G. Srajer, and G. De Stasio, J. Phys. Chem. A **107**, 2839 (2003).
[28] T. E. Westre, P. Kennepohl, J. G. DeWitt, B. Hedman, K. O. Hodgson, and E. I. Solomon, J. Am. Chem. Soc. **119**, 6297 (1997).
[29] D. Cabaret, Y. Joly, H. Renevier, and C. R. Natoli, J. Synchrotron Radiat. **6**, 258 (1999).
[30] M.-A. Arrio, S. Rossano, C. Brouder, L. Galoisy, and G. Calas, Europhys. Lett. **51**, 454 (2000).
[31] G. Drager, Th. Kirchner, S. Bocharov, and C. C. Kao, J. Synchrotron Radiat. **8**, 398 (2001).
[32] P. Glatzel and U. Bergmann, Coord. Chem. Rev. (to be published).
[33] G. Dräger, R. Frahm, G. Materlik, and O. Brummer, Phys. Status Solidi B **146**, 287 (1988).
[34] H. Heumann, G. Dräger, and S. Bocharov, J. Phys. IV **7**, C2-481 (1997).
[35] A. L. Ankudinov, B. Ravel, J. J. Rehr, and S. D. Conradson, Phys. Rev. B **58**, 7565 (1998).
[36] A. L. Ankudinov, C. E. Bouldin, J. J. Rehr, J. Sims, and H. Hung, Phys. Rev. B **65**, 104107 (2002).
[37] E. N. Maslen, V. A. Streltsov, N. R. Streltsova, and N. Ishizawa, Acta Crystallogr., Sect. B: Struct. Sci. **51**, 929 (1995).
[38] C. A. Francis and P. H. Ribbe, Am. Mineral. **65**, 1263 (1980).
[39] G. A. Novak and G. V. Gibbs, Am. Mineral. **56**, 791 (1971).
[40] D. R. Peacor and N. Niizeki, Z. Kristallogr. **119**, 98 (1963).
[41] S. D. Jacobsen, J. R. Smyth, R. J. Swope, and R. I. Sheldon, Am. Mineral. **85**, 745 (2000).
[42] K. Stahl and J.-P. Legros, Acta Crystallogr., Sect. B: Struct. Sci. **46**, 292 (1990).
[43] S. Lucchesi, U. Russo, and A. Della Giusta, Eur. J. Mineral. **9**, 31 (1997).
[44] R. I. Hill, J. R. Craig, and G. V. Gibbs, Phys. Chem. Miner. **4**, 317 (1979).
[45] T. Kohler, T. Armbruster, and E. Libowitzky, J. Solid State Chem. **133**, 486 (1997).
[46] S. Geller, Acta Crystallogr., Sect. B: Struct. Crystallogr. Cryst. Chem. **27**, 821 (1971).
[47] G. Lepicard and J. Protas, Bull. Soc. Fr. Mineral. Cristallogr. **89**, 318 (1966).
[48] C. Hoffman, T. Armbruster, and M. Kunz, Eur. J. Mineral. **9**, 7 (1997).
[49] W. Eventoff, R. Martin, and D. R. Peacor, Am. Mineral. **57**, 45 (1972).
[50] R. W. Cheary, Acta Crystallogr., Sect. B: Struct. Sci. **43**, 28 (1987).
[51] S. Turner and J. E. Post, Am. Mineral. **73**, 1155 (1988).
[52] J. E. Post and D. E. Appleman, Am. Mineral. **73**, 1401 (1988).
[53] J. E. Post and D. E. Appleman, Am. Mineral. **79**, 370 (1994).
[54] E. Chalmin, Ph.D. thesis, Université de Marne la Vallée, 2003 (in French).
[55] M. Wilke, F. Farges, P. E. Petit, G. E. Brown Jr., and F. Martin, Am. Mineral. **65**, 713 (2001).
[56] M. O. Krause and J. H. Oliver, J. Phys. Chem. Ref. Data **8**, 329 (1979).
[57] J. P. Rueff, L. Journel, P.-E. Petit, and F. Farges, Phys. Rev. B **69**, 235107 (2004).
[58] F. Farges, G. E. Brown Jr., and J. J. Rehr, Phys. Rev. B **56**, 1809 (1997).
[59] F. Farges, G. E. Brown Jr., M. Muñoz, and P. E. Petit, Geochim. Cosmochim. Acta **86**, 1665 (2001).
[60] F. Farges, Phys. Chem. Miner. **28**, 619 (2001).
[61] J. P. R. de Villers, Am. Mineral. **80**, 756 (1975).
[62] S. Turner and P. R. Buseck, Nature (London) **304**, 143 (1983).
[63] J. E. Post and D. R. Veblen, Am. Mineral. **75**, 477 (1990).
[64] B. Lanson, V. A. Drits, A.-C. Gaillot, E. Silvester, A. Plançon, and A. Manceau, Am. Mineral. **87**, 1631 (2002).
[65] A. Manceau, B. Lanson, and V. A. Drits, Geochim. Cosmochim. Acta **66**, 2639 (2002).
[66] F. Farges, S. Djanarthany, S. de Wispelaere, M. Munoz, B. Magassouba, H. Haddi, M. Wilke, C. Schmidt, M. Borchert, P. Trocellier, W. Crichton, A. Simionovici, P. E. Petit, M. Mezouard, M. P. Etcheverry, I. Pallot-Frossard, J. R. Bargar, G. E. Brown Jr., D. Grolimund, and A. Scheidegger, (unpublished).